

## Contact Line Stability and “Undercompressive Shocks” in Driven Thin Film Flow

A. L. Bertozzi,<sup>1</sup> A. Münch,<sup>1</sup> X. Fanton,<sup>2</sup> and A. M. Cazabat<sup>2</sup>

<sup>1</sup>*Departments of Mathematics and Physics, Duke University, Durham, North Carolina 27708*

<sup>2</sup>*Laboratoire de la Matière Condensée, Collège de France, 11 place Marcelin-Berthelot, 75231 Paris Cedex 05, France*

(Received 4 August 1998)

We present new experimental results for films driven by a thermal gradient with an opposing gravitational force. When the gravitational effect becomes non-negligible, the advancing front produces a very large capillary ridge which shows a remarkable tendency to remain stable. This phenomenon can be explained by new mathematical results for a lubrication model of the experiment. The advancing front evolves into an “undercompressive” capillary shock structure which is stable to contact line perturbations, unlike typical capillary ridges in driven film flows. [S0031-9007(98)07868-5]

PACS numbers: 68.15.+e, 03.40.Gc, 47.20.Ma, 68.45.Gd

We consider a film driven by a thermal gradient with a counteracting gravitational force. For very thin capillary driven films, previous experiments [1,2] show that the Marangoni stress causes a capillary ridge to form and the film to finger (see Fig. 1), via a very similar process to that observed in gravitationally driven films [3]. Earlier experiments [4] for thicker Marangoni films balanced by gravity, showed that no bump or capillary ridge was present near the contact line and the front was relatively stable.

We find that there is a rather unusual transition from the case of thinner films. A very large capillary ridge forms; however, the ridge continues to broaden as it advances up the plate. At the same time, the speed of the front is slower than that predicted in [2]. Despite the large capillary ridge, the contact line remains stable.

Using a lubrication model, we show that this observed transition is due to a fundamental change in structure of the front, from a classical capillary shock (for negligible gravity), which is linearly unstable to perturbations, to a double shock structure (for non-negligible gravity) with an “undercompressive (UC) shock” [5], which is linearly stable to perturbations, as the leading front. The undercompressive structure also manifests itself in larger bumps that continue to broaden, a feature also observed in the experiment. This is the first case where we are aware of a physical system exhibiting an undercompressive shock associated with a scalar hyperbolic conservation law.

*Experimental results.*—A liquid film is driven from a macroscopic reservoir onto a tilted plate by a surface tension gradient, induced by a constant temperature gradient externally imposed along the plate. The liquid is a nonvolatile polydimethylsiloxane (PDMS) from Petrarch, dynamic viscosity  $\eta = 0.0965$  Pa s, surface tension  $\gamma = 0.0209$  N m<sup>-1</sup>, density  $\rho = 965$  kg/m<sup>3</sup> (at 25 °C), which completely wets the substrate. The substrate plate is an oxidized silicon wafer, first put into contact with PDMS, then cleaned with hexane and rinsed with methanol before use. The cleaning procedure gives very reproducible surfaces, quite insensitive to contamination due to the remaining 7-Å-thick monolayer of PDMS. Note that this sets a

length scale for the precursor layer in the model of the next section.

To increase the film thickness to the scale of 10  $\mu\text{m}$ , we tilt the plate at an angle from the vertical. Capillarity (and therefore the curvature of the meniscus between the reservoir and the film) still plays a role in the value of the film thickness in this range, allowing us to control the film by a geometrical parameter [6], as opposed to increasing the thermal gradient, which would ultimately lead to nonlinear behavior of the fluid. See Fig. 2 in Ref. [6(a)] for a diagram of the apparatus.

Our experimental results are quite unexpected: with increasing  $h_\infty$  (the thickness of the flat part of the film) we observe that the bump becomes more pronounced, but that the contact line becomes stable. Figure 2 shows the shape of the entire contact line at the end of the experiment for thicker films. The second picture, corresponding to a film height of 11  $\mu\text{m}$ , showed no contact line corrugation. However, the profile of the film, shown in Fig. 3 via (+), shows that the film has a rather large pronounced bump. Moreover, no stationary state is reached, and the bump continues to widen with time. In addition, Fig. 4 shows the discrepancy between the experimentally measured speed of the front (shown as circles) and the theoretical front

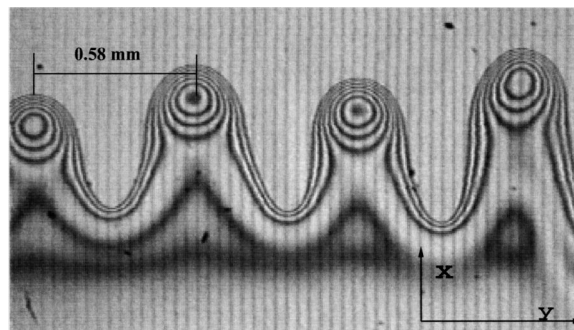


FIG. 1. Film thickness of 0.6  $\mu\text{m}$  ( $h_\infty = 0.02$ ), surface tension gradient  $\tau = 0.18$  Pa,  $\alpha = 90^\circ$ . Equal-thickness interference fringes are used to reconstruct thickness profiles, as in Fig. 3.



FIG. 2. Top: Film thickness of  $4 \mu\text{m}$ ,  $\tau = 0.19 \text{ Pa}$ ,  $\alpha = 35^\circ$ ; the contact line is almost stable ( $h_\infty = 0.075$ ). Bottom: Film thickness of  $11 \mu\text{m}$ ,  $\tau = 0.11 \text{ Pa}$ ,  $\alpha = 20^\circ$ ; the contact line is stable ( $h_\infty = 0.21$ ). In both cases, the distance between the two vertical bars is  $25 \text{ mm}$ .

speed [2,6] (solid line) as a function of upstream film height.

*The model.*—We use a lubrication model with a “depth averaged” velocity [2,6]

$$\vec{V} = \left( \frac{\tau h}{2\eta} - \frac{\rho g h^2 \sin \alpha}{3\eta} \right) \vec{e}_x + \frac{\gamma h^2 \nabla^3 h}{3\eta}, \quad (1)$$

where  $\tau$  denote the surface tension gradient,  $\alpha$  the angle of inclination (from the horizontal) of the plane,  $g$  the gravitational constant,  $\rho$ ,  $\eta$ , and  $\gamma$  are as in the section “Experimental results,” and  $x$  is along the direction of the flow, parallel to the plate. The coefficient of  $\vec{e}_x$  in the expression for  $\vec{V}$  represents convection of the film due to surface tension gradient and due to the component of gravity tangent to the surface. For the range of parameters considered in these experiments, the component of gravity normal to the surface had a negligible effect on the dynamics, so we ignore it here.

We now couple this equation with conservation of mass,  $h_t + \nabla \cdot (h\vec{V}) = 0$ . To first understand the dynamics of the front, we ignore until the section “Stability of the front” the effects of perturbations in the direction  $y$  transverse to the direction of flow and consider solutions  $h$  depending only on  $x$  and  $t$ :

$$h_t + (f(h))_x = - \left( \frac{\gamma h^3 h_{xxx}}{3\eta} \right)_x, \quad (2)$$

where the flux satisfies  $f(h) = (\tau h^2/2 - \sin \alpha \rho g h^3/3)/\eta$ .

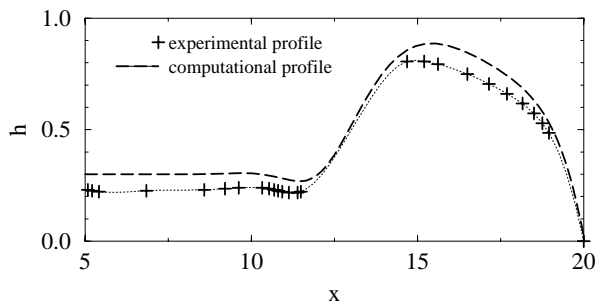


FIG. 3. Experimental profile (+) in the dimensionless units, at  $t = 215$  with  $h_\infty = 0.21$ . The thicknesses are determined by following the fringes from the relatively smooth profile at the edge of the wafer, where they are easier to count. The dashed line shows the numerical profile of a simulation of (3) with  $b = 0.005$ ,  $h_\infty = 0.3$ , taken at  $t = 210$ .

To rescale (2), consider length scales  $H$ ,  $l$ , and a corresponding time scale  $T$ :  $h = H\hat{h}$ ,  $x = \hat{x}l$ , and  $t = T\hat{t}$ . Balancing the competing convective effects of gravity and Marangoni forces in  $f(h)$  gives  $H = \frac{3\tau}{2\sin \alpha \rho g}$ . Setting  $l$  to be the capillary length on which surface tension balances the driving forces on the left-hand side of (2) gives  $l = \left( \frac{3\gamma\tau}{2\rho^2 g^2 \sin^2 \alpha} \right)^{1/3}$ . The time scale is such that all three of these effects balance,  $T = 2\frac{\eta}{\tau^2} \left( \frac{4}{3} \tau \gamma \rho g \sin \alpha \right)^{1/3}$ . Dropping the  $\hat{\cdot}$  notation gives the dimensionless equation

$$h_t + (h^2 - h^3)_x = -(h^3 h_{xxx})_x. \quad (3)$$

In the experiment, there is a front of fluid that connects to a flat film upstream (to the left in Fig. 3), with thickness determined by the dynamics of the meniscus. In the model, we take that film thickness as a given constant height  $h_\infty$  upstream (as  $x \rightarrow -\infty$ ). We choose the simplest boundary condition consistent with complete wetting, that of a precursor model in which  $h \rightarrow b > 0$  as  $x \rightarrow \infty$  [7,8]. Moving fronts of nonvanishing velocity have a precursor film of molecular dimensions [9]. Thus we take  $b$  to be a positive, albeit extremely small, value to avoid the well-known paradox associated with a moving contact line.

*Lax and undercompressive shocks.*—Neglecting, for the moment, the effects of curvature, (3) reduces to the scalar hyperbolic conservation law  $h_t + (f(h))_x = 0$  where  $f$  is the nonconvex flux function  $h^2 - h^3$ . Smooth solutions are easily computed via the method of characteristics:  $h(x, t) = h_0(x - f'(h(x, t))t)$ . In addition, there are solutions with propagating discontinuities (shocks)

$$h(x, t) = \begin{cases} h_-, & x < x_0 - st, \\ h_+, & x \geq x_0 - st, \end{cases} \quad (4)$$

$$s(h_-, h_+) = \frac{f(h_-) - f(h_+)}{h_- - h_+},$$

which correspond to advancing fronts when the effects of curvature are included. The shock is called *compressive*

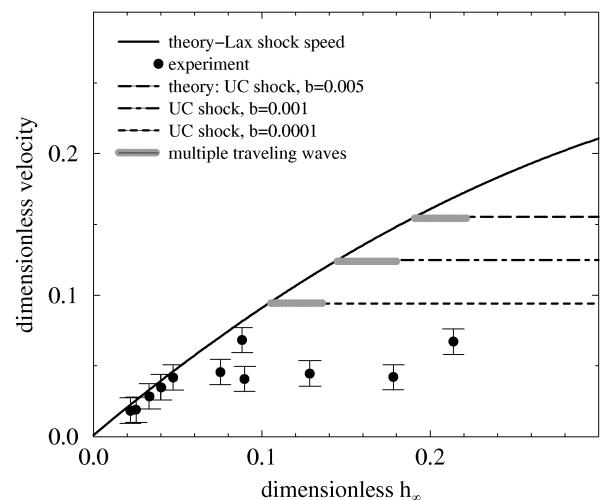


FIG. 4. The speed of the front vs upstream film thickness,  $h_\infty$ .

or a *Lax shock* if it satisfies the entropy condition [10]

$$f'(h_+) < s < f'(h_-). \quad (5)$$

Such shocks are the only admissible ones in the  $\epsilon \rightarrow 0$  limit of  $h_t + (f(h))_x = \epsilon h_{xx}$  [11]. Shocks violating condition (5) are called *undercompressive* and are known to arise in equations with nonconvex fluxes and combined diffusive and dispersive effects [12]. For nonconvex fluxes, compressive shocks connect states on the graph of the flux function via a chord that does not cross the graph of the flux. Undercompressive shocks, on the other hand, connect states via a chord that crosses the flux function. In the case of a compressive shock, characteristics enter the shock from both sides, while for an undercompressive shock, the characteristics enter only on one side.

The admissibility of a particular shock with left and right states  $h_-$  and  $h_+$  is determined by the existence of a traveling wave solution  $h_{tr}(x - st)$  of the full system, in our case Eq. (3), connecting the state  $h_- = \lim_{\xi \rightarrow -\infty} h_{tr}(\xi)$  to the state  $h_+ = \lim_{\xi \rightarrow \infty} h_{tr}(\xi)$ . We call such a wave either a “capillary Lax shock” or “undercompressive capillary shock” depending on the structure of the discontinuity in the underlying hyperbolic problem.

We now briefly summarize recent results in [5] on the existence of capillary shocks for (3). If we let  $h_+ = b \ll 1$  then we find that (i) for  $h_-$  small, near  $b$ , there exists a unique capillary Lax shock connecting  $h_-$  to  $b$ . (ii) For larger values of  $h_-$  there are two thresholds  $h_1(b)$  and  $h_2(b)$  so that for  $h_1 < h_- < h_2$  there exist more than one capillary Lax shock connecting  $h_-$  to  $b$ . Within this range, there is a special value  $h_* \in (h_1, h_2)$  for which there exists an infinite number of capillary Lax shocks connecting  $h_*$  to  $b$ . (iii) For  $h_- > h_2$ , there are no capillary Lax shocks connecting  $h_-$  to  $b$ . (iv) However, there is a special value, which we denote by  $h_{uc}(b)$ , which is typically significantly larger than  $h_2$ , for which there exists a single undercompressive capillary shock. The undercompressive shock height  $h_{uc}$  is related to  $h_*$  by the formula  $h_{uc} = 1 - h_* - b$ . On the graph of the flux function  $f$ , the chord connecting  $b$  to  $h_*$  extends upwards to intersect the flux function again at  $h_{uc}$ . This undercompressive shock travels with the same speed  $s_*(b) := s(h_{uc}, b) = s(h_*, b)$  as the infinite family of Lax shocks connecting  $h_*$  to  $b$ . Moreover, it is the limiting shape of the infinite family of Lax shocks connecting  $h_*$  to  $b$ . It is interesting to note that the capillary Lax shocks always have a capillary ridge or bump at the leading edge of the shock while the undercompressive shock has no bump.

The undercompressive capillary shock plays an important role in the dynamics of solutions of Eq. (3). If we take the initial condition to be a slightly smoothed shock of the form (4) at  $t = 0$ , with  $h_+ = b$  and  $h_- = h_\infty$ , the evolution of the solution of (3) depends dramatically on how  $h_\infty$  compares to the special values  $h_1$ ,  $h_2$ , and  $h_{uc}$ . For  $h_\infty < h_1$  we always observe rapid convergence to the unique capillary Lax shock. For  $h_1 < h_\infty < h_2$  the jump

initial condition typically evolves into the capillary Lax shock with the smallest bump. For  $h_{uc} > h_\infty > h_2$ , the solution always evolves into a double shock structure with a leading undercompressive capillary shock connecting  $h_- = h_{uc}$  to  $h_+ = b$  and a trailing capillary Lax shock connecting  $h_- = h_\infty$  to  $h_+ = h_{uc}$  [13]. The speed  $s$  of each shock, given by the formula in (4), can be seen graphically as the slope of the chord connecting the left and right states on the graph of the flux function  $f$  (see [5] for examples). The trailing shock moves with a slower speed than the leading shock. This is necessary in order for the two to separate. Note also that the advancing undercompressive shock travels with a slower speed than would a single Lax shock (if it existed) connecting the states  $h_\infty$  to  $b$  (see Fig. 5).

This slower front speed is the signature of the undercompressive shock that we measure in the experiment (see Fig. 4). The solid dark line is the dimensionless Lax shock speed  $s$  as a function of  $h_\infty$ . Here we assume  $b$  is very small so we approximate  $s$  by  $h_\infty - h_\infty^2$ . The undercompressive shock speed  $s_*(b)$  is shown via horizontal dashed lines for several values of  $b$  (0.005, 0.001, and 0.0001). Note that these horizontal lines intersect the Lax shock speed curve at the value  $h_*(b)$ . The thick grey bars denote, for each value of  $b$ , the range  $h_* < h < h_2$ . Above  $h_2$ , the only possible dynamics is that of a double shock structure with the undercompressive shock as the leading front. The experimental data show that for very thin films the front speed is in extremely good agreement with the Lax shock speed from the theory. For thicker films the front speed is essentially independent of film thickness  $h_\infty$ , and is much slower than the Lax shock speed. This is the expected behavior for an undercompressive shock. The experimental front speeds are even slower than the UC shock with  $b = 0.0001$ , suggesting an experimental  $b$  that is very small. This is consistent with the idea that advancing fronts see only a precursor thickness of molecular dimensions.

Figure 3 shows the experimental thickness profile of the film corresponding to the experiment in series 2 with the largest film height  $h_\infty = 0.21$ . We cannot accurately compute solutions of (3) with  $b < 10^{-3}$ , but our numerics

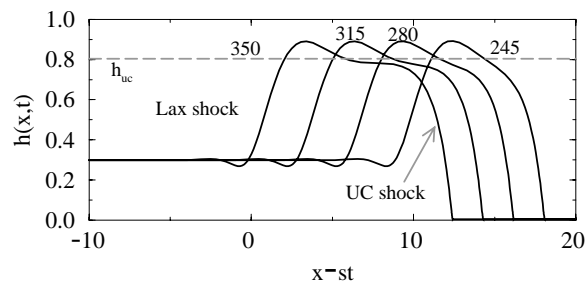


FIG. 5. The numerical profiles ( $b = 0.005$ ,  $h_\infty = 0.3$ ) at later times 245, 280, 315, and 350. The reference frame moves with the speed  $s = s(h_\infty, b) > s_*$ .

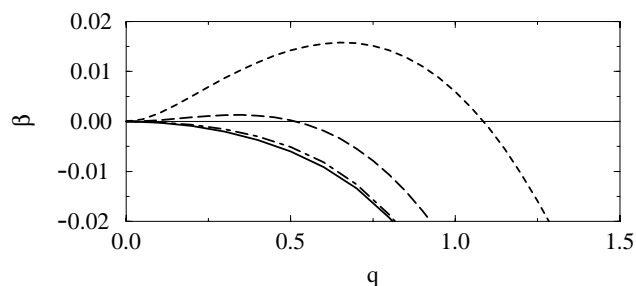


FIG. 6. The two upper dashed lines correspond to the (smallest) capillary Lax shock for  $h_- = h_*(b)$  and  $b = 0.01$  (short-dashed line) and  $b = 0.1$  (long-dashed line). The range of positive  $\beta$  in both plots indicates a long-wave instability. The lower curves (dot-dashed line:  $b = 0.1$ ; solid line:  $b = 0.01$ ) correspond to the undercompressive front of the double shock, connecting  $h_- = h_{uc}(b)$  to  $h_+ = b$ .

indicate that the shape of the separating fronts are rather insensitive to the particular choice of  $b$ . The time scale of the separation of the shocks depends on the differences in the front speeds which is (to leading order) determined by  $h_\infty - h_*(b)$ . In the experiment, Fig. 4 indicates  $h_\infty - h_*(b) \sim 0.11$ ; to obtain a similar time scale of separation with a different choice of  $b$ , for example,  $b = 0.005$ , we increase  $h_\infty$  to the value 0.3. The simulation of (3) starts with the jump initial condition (4) at  $t = 0$ . The numerical profile at  $t = 210$  is shown in Fig. 3 as a dashed line; the shape is almost identical to the profile in the experiment at roughly the same dimensionless time. If we compute past this time (see Fig. 5), the profile separates clearly into a leading undercompressive shock, moving with speed  $s_*$ , and a trailing Lax shock, moving with speed  $s(h_{uc}, h_\infty)$ . We expect that future experiments could observe further separation of the fronts as shown in Fig. 5.

*Stability of the front.*—Linear stability of the front for very thin films and very thick films was considered in [14]. For intermediate thickness films, we compare the stability of the Lax shock profiles for  $h_\infty$  near  $h_*(b)$  and contrast this to the stability of the leading front (UC shock) in the double shock structure for slightly thicker films.

To study stability, we consider perturbations of the front as a solution of the two dimensional model

$$h_t + (f(h))_x = -\nabla \cdot (h^3 \nabla^3 h). \quad (6)$$

For perturbation of the form  $\delta g(x)e^{\beta t + i q y}$  we linearize (6) about the respective traveling wave solution and compute the largest eigenvalue  $\beta$  as a function of  $q$ . We use the same method as in [7] and the results are shown in Fig. 6. The curves clearly show that the capillary Lax shocks for smaller  $h_\infty$  are linearly unstable; however, the undercompressive capillary shock, describing the leading front of the double shock with larger  $h_\infty$ , is linearly stable. This explains the stability of the contact line observed in the experiment (see Fig. 2).

We thank M. Brenner, P. G. de Gennes, and M. Shearer for useful conversations. A.B. and A.M. are supported by a PECASE award administered by the U.S. Office of Naval Research. X.F. is supported by CNRS BDI Grant No. 1000881.

- [1] A.M. Cazabat *et al.*, Nature (London) **346**, 824 (1990).
- [2] P. Carles and A.M. Cazabat, J. Colloid. Interface Sci. **157**, 196 (1993).
- [3] H. Huppert, Nature (London) **300**, 427 (1982); J.R. de Bruyn, Phys. Rev. A **46**, R4500 (1992).
- [4] V. Ludviksson and E.N. Lightfoot, AIChE J. **17**, 1166 (1971).
- [5] A.L. Bertozzi, A. Münch, and M. Shearer (to be published).
- [6] (a) X. Fanton, A.M. Cazabat, and D. Quéré, Langmuir **12**, 5875 (1996); (b) X. Fanton, Ph.D. thesis, Université Pierre et Marie Curie, Paris, 1998.
- [7] A.L. Bertozzi and M.P. Brenner, Phys. Fluids **9**, 530 (1997).
- [8] S.M. Troian *et al.*, Europhys. Lett. **10**, 25 (1989).
- [9] P.G. de Gennes, Rev. Mod. Phys. **57**, 827 (1985).
- [10] P.D. Lax, *Hyperbolic Systems of Conservation Laws and the Mathematical Theory of Shock Waves*, CBMS-NSF Regional Conference Series in Applied Math Vol. 11 (SIAM, Philadelphia, 1973).
- [11] O. Oleinik, Usp. Mat. Nauk. **14**, 165–170 (1959).
- [12] B. Hayes and M. Shearer, Proc. R. Soc. Edinburgh Sect. A (to be published).
- [13] For  $h_\infty > h_{uc}$  the solution evolves via a combination rarefaction-undercompressive shock [5]. Unlike the classical rarefaction shock introduced in [4], the UC shock separates from the rarefaction fan.
- [14] D.E. Kataoka and S.M. Troian, J. Colloid Interface Sci. **192**, 350 (1997); **203**, 335 (1998).